On Discrete-Time Modeling of the Filtered and Symbol-Rate Sampled Continuous-Time Signal affected by Wiener Phase Noise

S. Mandelli[a], M. Magarini[a,*], A. Spalvieri[a], S. Pecorino[a]

[a]*Dipartimento di Elettronica, Informazione e Bioingegneria, Politecnico di Milano, Piazza L. da Vinci 32, Milan 20133, Italy*

Abstract

This paper investigates the differences between the symbol-spaced discrete-time Wiener phase noise channel model, commonly assumed in the literature to represent the effect of phase noise, and that obtained by symbol-rate sampling the filtered continuous-time received signal affected by **continuous-time** Wiener phase-noise. In particular, for comparison, we consider some statistical tests to check temporal and distributional properties of the two models. We show that the fit between the two models is very good even for quite strong values of phase noise. The main result is that when the standard deviation of the discrete-time Wiener phase noise increment σ_{PN} is below a threshold of approximately $\bar{\sigma}_{PN} \simeq 0.1$ rad, **the discrete-time Wiener model** provides a good approximation to the actual symbol-spaced sampled filtered signal **affected by continuous-time Wiener phase noise**. We show that when σ_{PN} is below $\bar{\sigma}_{PN}$ the ratio between the power of the signal and the power of the model mismatch is greater than 20 dB. Simulation results are also presented to compare bit error rates of the two models in case of QPSK and 16-QAM transmission and to compare the power spectral densities of their associated complex exponential phase noises. Our results suggest that the discrete-time Wiener phase noise model can be adopted for many real-world systems, where, according to experimental results available in the literature, σ_{PN} in the order of 0.1 rad is rarely found even when the nonlinearity of the optical channel is deeply stressed.

Keywords: Optical communication, coherent detection, phase noise, quadrature amplitude modulation (QAM), quadrature phase-shift keying (QPSK).

---

*Corresponding author

Email addresses: silvio.mandelli@polimi.it (S. Mandelli), maurizio.magarini@polimi.it (M. Magarini), arnaldo.spalvieri@polimi.it (A. Spalvieri), simone.pecorino@polimi.it (S. Pecorino)

1. Introduction

Multiplicative phase noise is one of the major impairments affecting the performance of coherent optical transmission systems [1–3]. Phase noise is due to both laser oscillators used for up- and down-conversion [4], and to cross-phase modulation that arises in wavelength-division-multiplexing systems [5]. A recent tutorial on transmission over phase noise channels is [6].

Several schemes have been proposed to estimate the received carrier phase for arbitrary PSK and QAM constellations in presence of phase noise. **Among *blind* methods, the feedforward scheme of [7] addresses the constraints imposed by high speed parallel processing, while in [8] the performance of Viterbi-Viterbi carrier phase estimation is investigated for circular QAM signals.** Pilot-aided carrier phase recovery schemes have recently gained attention as candidate phase recovery approaches for systems affected by strong phase noise. Papers [9, 10] are based on the insertion of a pilot tone in a notch of the transmitted signal spectrum, while in papers [11–13] pilot symbols are inserted in time domain. Papers [14–19] discuss coding and demodulation techniques based on pilot symbols aimed at combating the cycle-slip phenomenon. Also, schemes based on time domain interleaving of robust modulation formats and less robust, but more spectrally efficient modulation formats, are proposed in [20, 21]. The information rate transferred through the discrete-time phase noise channel is studied in [22–26] while that associated with multiple-input multiple-output channels is considered in [27, 28].

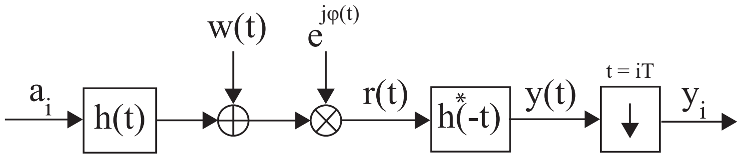

Figure 1: Complex baseband representation of the transmission system with multiplicative phase noise, matched filtering, and symbol-rate sampling.

With reference to Fig. 1, the complex baseband model of the continuous-time signal $r(t)$ at the input of the receiver is

$$r(t) = \sum_{l} a_l h(t - lT) e^{j\varphi(t)} + w(t) e^{j\varphi(t)}, \tag{1}$$

where $\{a_i\}$ is the sequence of zero-mean complex symbols with unit variance $\sigma_a^2 = 1$ transmitted at rate $1/T$, $j = \sqrt{-1}$ is the imaginary unit, $h(t)$ is the square-root Nyquist impulse response of the transmit shaping filter with energy E_h and $w(t)$ is the complex Additive White Gaussian Noise (AWGN) with power spectral density N_0. The signal-to-noise ratio is SNR=E_s/N_0, **where $E_s = \sigma_a^2 E_h$ is the average energy per symbol.** The information rate between the input modulation and the continuous-time signal of eq. (1) is studied in [29, 30] **while a lower bound on the capacity has been recently derived**

in [31]. Upper bounds on the SNR penalty due to phase noise with arbitrary discretization in time domain are given in [32]. In [4] it is shown that phase noise introduced by laser oscillators can be modeled as a continuous-time Wiener process. The random phase of a continuous-time Wiener process evolves as

$$\varphi(t) = \varphi(0) + \sigma \int_0^t \lambda(\tau) d\tau, \tag{2}$$

where $\varphi(0)$ is uniform in $[-\pi, \pi)$, σ is a real constant, and $\lambda(t)$ is a white Gaussian process with autocorrelation

$$E\left[\lambda(\tau)\lambda(\tau + t)\right] = \delta(t),$$

where $\delta(t)$ is the Dirac delta function and $E[\cdot]$ is the expectation. For Wiener phase noise, the power spectral density of the complex exponential $e^{j\varphi(t)}$ is known to be **the Lorentzian function given by [33]**

$$\mathcal{L}(f) = \frac{4\sigma^2}{\sigma^4 + 16\pi^2 f^2} \tag{3}$$

with 3 dB linewidth $\sigma^2/(4\pi)$.

However, processing the continuous-time signal, or a finely time-discretized version of it, is too complex, therefore in the practice processing is made on the symbol spaced sampled complex sequence after the matched filter, that is sequence $\{y_i\}$ in Fig. 1. The discrete-time model

$$\tilde{y}_i = a_i e^{j\varphi_i} + n_i \tag{4}$$

is adopted in the bibliography on discrete-time phase noise channel as an approximation to the actual sampled signal $y_i = y(iT)$, with $\varphi_i = \varphi(iT)$. The discrete-time Wiener phase noise process is described as

$$\varphi_i = \varphi_{i-1} + \sigma_{PN}\lambda_i, \tag{5}$$

where $\sigma_{PN}^2 = \sigma^2 T$ and λ_i is an i.i.d. discrete-time Gaussian random process with zero mean and unit variance; **the term $\sigma_{PN}\lambda_i$ can be interpreted as the instantaneous value of a white frequency noise process, being it given by the difference between two successive phase noise samples**. In other words, translation from continuous to discrete-time is simply obtained by neglecting the effects of the receive filter on the multiplicative phase noise.

The model defined by (4) and (5) is commonly assumed in computer simulations for bit-error rate (BER) evaluation. Remarkably, the experimental results presented in [34] show that the model in (4) and (5) can be adopted to describe carrier phase noise after nonlinear propagation in different transmission scenarios. **From now on** the actual sequence $\{y_i\}$ of (1) **will be denoted as** Continuous-Time Wiener Sampled Matched Filter (CTWSMF) model, while the approximation $\{\tilde{y}_i\}$ to the actual $\{y_i\}$ **will be referred as Discrete-Time Wiener (DTW) model.** The aim of this paper is to show what are the limits of applicability of the DTW for approximating the CTWSMF. In order to do this, we perform statistical tests on temporal and distributional properties of CTWSMF **for two different roll-offs that can be considered as end-points of the range of values that are of practical interest in optical systems** and compare them with those performed on the DTW model. The main result is the proof, by simulations, that DTW is a good approximation of the CTWSMF when $\sigma_{PN} < 0.1\,\text{rad}$. As a further way of evaluating the accuracy provided by the approximation we present computer simulations to compare BERs of QPSK and 16-QAM and the power spectral densities of the complex exponential phase noise obtained by using the two models.

The paper is organized as follows. Section 2 contains the mathematical derivation of the CTWSMF and suggests a frequency domain interpretation of the mismatch between CTWSMF and DTW. Sections 3 and 4 go further in depth by comparing the statistical characterizations of the discrete-time sampled-spaced output signals and by discussing the mismatch between the two models. Simulation results are presented in Sec. 5, where we compare the BER and the power spectral density of discrete time phase noise with CTWSMF and with its DTW approximation. Finally, conclusions are drawn in Sec. 6.

2. Continuous-time Wiener Sampled Matched Filter Model

The signal $r(t)$ in (1) is filtered through the square root Nyquist matched filter $h^*(-t)$ and sampled at the time instants $t = iT$, obtaining

$$y_i = \sum_{l=-\infty}^{\infty} a_{i-l} c_l^{(i)} + n'_i, \tag{6}$$

where

$$c_l^{(i)} = \int_{-\infty}^{+\infty} h(\tau - lT) h^*(\tau - iT) e^{j\varphi(\tau)} d\tau \tag{7}$$

and

$$n'_i = \int_{-\infty}^{\infty} w(\tau) e^{j\varphi(\tau)} h^*(\tau - iT) d\tau.$$

If the phase noise cannot be approximated as nearly constant within the effective duration of the impulse response of the receive filter, the Nyquist condition for Inter-Symbol Interference (ISI) free transmission is not satisfied. It is worth writing the output of the sampled matched filter as

$$y_i = a_i e^{j\varphi'_i} \cdot \rho'_i + n'_i. \tag{8}$$

Equation (8) defines the CTWSMF. By comparing the CTWSMF to the DTW of (4) one observes that:

- the additive noise n'_i is statistically equivalent to the additive noise n_i of the DTW model;

- the term $\rho_i' e^{j(\varphi_i'-\varphi_i)}$ is a distortion on the symbol a_i given by the integration of the complex exponential through the matched filter. Actually, as pointed out in [4], since the effect of filtering is to convert phase fluctuations in amplitude variations, phase noise can have a detrimental effect not only for the case of phase modulations (PMs) but also in that of amplitude modulations (AMs), but the PM-AM conversion is totally neglected in the DTW.

The distortion term can be explained also by reasoning in frequency domain. The noiseless part of the received signal $r(t)$ in (1) corresponds to the multiplication of the filtered data sequence with $e^{j\varphi(t)}$. If one translates this to the frequency domain the power spectral density of the noiseless part of the received signal is the convolution between $\sigma_a^2|H(f)|^2/T$ and the Lorentzian spectrum of the complex exponential phase noise given in (3). Since the overall frequency response from the input of the transmit filter to the output of the matched filter is not proportional to $|H(f)|^2$, ISI arises.

3. Modeling the CTWSMF Phase Noise

We want to check if φ_i' appearing in eq. (8) is a discrete-time Wiener process or not, hence if it can be approximated as φ_i of (4). To achieve this, we must verify that

$$\upsilon_i = \varphi_i' - \varphi_{i-1}', \tag{9}$$

is a white Gaussian random variable. Being υ_i the difference between two phases at the two successive time instants iT and $(i-1)T$ we name it Discrete-Time Frequency Noise (DTFN). In the following, the AWGN terms n_i and n_i' appearing in (4) and (8) will be neglected because they affect the two discrete-time models in the same way. We denote the noiseless part of the symbol-spaced signal at the output of the receive matched filter in (8) as

$$x_i = a_i e^{j\varphi_i'} \cdot \rho_i'. \tag{10}$$

The analysis of the mismatch between CTWSMF and DTW is performed by means of simulations. **It is worth emphasizing that since the goal of this study is to analyze the non-linear effects introduced by phase noise, time-domain processing is implemented.** In order to synthetically generate the actual signal y_i in (8) the continuous-time signal is sampled at a rate much higher than the symbol interval. In our simulations the oversampling factor is equal to 20. **Such a value has been chosen after a preliminary analysis with the goal of providing a safe margin for aliasing free processing and, at the same time, obtaining numeric results with reasonable complexity.** The discrete-time signal sequence $\{\upsilon_i\}$ given in (9) is generated as shown in Fig. 2.

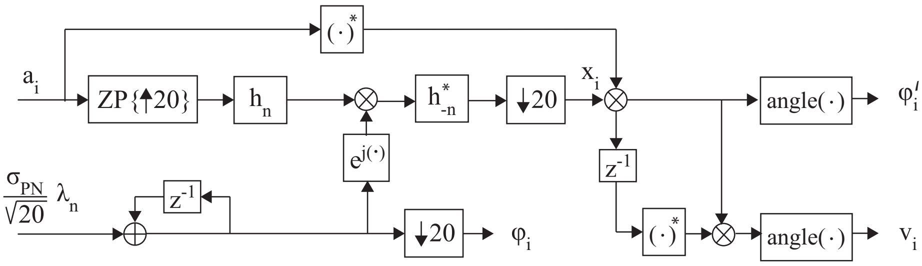

Figure 2: Block diagram for the generation of υ_i, φ_i and φ_i'. The block ZP ($\uparrow$20) appends 19 zeros after one valid sample (up-sampling with zero-padding). The block $\downarrow$20 performs decimation (down-sampling) by a factor 20 to extract samples at integer multiples of the symbol interval. The discrete-time impulse response h_n is obtained by oversampling $h(t)$ at 20 times the symbol frequency while the oversampled discrete-time random process λ_n is i.i.d. with zero mean and unit variance.

3.1. Test of Whiteness

In the test of whiteness we focus on the estimation of the DTFN autocorrelation. In particular we consider the Pearson's Correlation Coefficient (PCC) with time lag lT

$$\mathrm{PCC}_l = \frac{\mathrm{Cov}[\upsilon_i \upsilon_{i+l}]}{\sigma_\upsilon^2}, \tag{11}$$

where σ_υ^2 is the variance of υ_i and $\mathrm{Cov}[\upsilon_i \upsilon_{i+l}] = E[\upsilon_i \upsilon_{i+l}] - E^2[\upsilon_i]$ is the covariance between random variables υ_i and υ_{i+l}. **Pearson's correlation coefficient is one of the most popular tests for measuring the linear dependence between two continuous random variables [35]. From (11) it follows that PCC_l is always comprised between -1 and $+1$. Specifically, while a value of PCC_l equal to 0 means that there is no correlation between the two random variables, a value of $+1$ (-1) means that there is a perfect positive (negative) relationship between them and, therefore, as one variable increases, the second variable increases (decreases) in exactly the same proportion.** When the DTFN sequence υ_i is white it happens that

$$\mathrm{PCC}_l = \begin{cases} 1, & \text{if } l = 0, \\ 0, & \text{otherwise.} \end{cases} \tag{12}$$

A sequence of N DTFN samples $\{\upsilon_1, \upsilon_2, ..., \upsilon_N\}$, generated by simulation, is used for obtaining an estimate of the mean and of the expected values in (11). The mean is estimated as

$$\mathrm{E}[\upsilon_i] \simeq \hat{m}_\upsilon = \frac{1}{N} \sum_{i=1}^{N} \upsilon_i. \tag{13}$$

while the unbiased estimate of $\mathrm{E}[\upsilon_i \upsilon_{i+l}]$ is

$$\mathrm{E}[\upsilon_i \upsilon_{i+l}] \simeq \frac{1}{N-l-1} \sum_{i=1}^{N-l} \upsilon_i \upsilon_{i+l}. \tag{14}$$

The unbiased estimate of the DTFN variance turns out to be

$$\hat{\sigma}_{\upsilon}^2 = \frac{1}{N-1} \sum_{i=1}^{N} (\upsilon_i - \hat{m}_{\upsilon})^2. \tag{15}$$

By putting (13), (14) and (15) in (11) we get the Estimated PCC_l as

$$\mathrm{EPCC}_l = \frac{N-1}{N-l-1} \frac{\sum_{l=1}^{N-l} (\upsilon_i - \hat{m}_{\upsilon})(\upsilon_{i+l} - \hat{m}_{\upsilon})}{\sum_{i=1}^{N} (\upsilon_i - \hat{m}_{\upsilon})^2}. \tag{16}$$

From the simulations we found $\hat{m}_{\upsilon} \simeq 0$.

Figures 3 and 4 show EPCC_1 and EPCC_2, respectively, versus σ_{PN} for QPSK and 16-QAM with roll-off $\alpha = 0.1$ and $\alpha = 0.5$. **These two roll-offs can be considered as the endpoints of the range of values that are of practical interest for optical systems.** In Fig. 3 we see that **for both the two considered modulation formats** the value of EPCC_1 is between 0.2 and 0.28 for σ_{PN} lower than 0.3 rad while it approaches zero for higher values of σ_{PN}. **Concerning** EPCC_2**, from Fig. 4 one realizes that while for** $\alpha = 0.5$ **its value is always around** 0 **for all the values of** σ_{PN}**, for** $\alpha = 0.1$ **its value is around** 0.04 **for** σ_{PN} **lower than** 0.3 **rad and then it decreases to** 0 **for higher values of** σ_{PN}**. However, independently on the roll-off value and modulation type,** $\mathbf{EPCC}_2$ **can be considered negligible with respect to** $\mathbf{EPCC}_1$**. Other values** EPCC_l**, with** $l > 2$**, are not reported, since** $\mathrm{EPCC}_l \simeq 0$**.**

From the numerical results presented in Figs. 3 and 4 we can clearly distinguish between two different cases: the first where σ_{PN} **is lower than** 0.3 **rad and the second where it is higher. In the first case we see that while for** $\alpha = 0.5$ **the values of** $\mathbf{EPCC}_1$ **and** $\mathbf{EPCC}_2$ **are virtually not affected by the modulation format, for** $\alpha = 0.1$ **this property is satisfied only by** $\mathbf{EPCC}_2$**. Concerning with** $\mathbf{EPCC}_1$**, a higher value can be observed for QPSK than for** 16**-QAM. A possible explanation of this behavior resides in the combined effect of different amplitude levels of** 16**-QAM and slow-decaying tails of the Nyquist impulse responses with small roll-off values. The fast amplitude variations within a symbol interval induced by higher tails and amplitude levels of** 16**-QAM interfere in a stronger way thus reducing the observed correlation between successive samples of** υ_i**. In the second case, where** σ_{PN} **has values higher than** 0.3 **rad, we can see that the large phase change occurring between successive samples of the phase noise Wiener random process totally decorrelates the sequence of samples** υ_i**.**

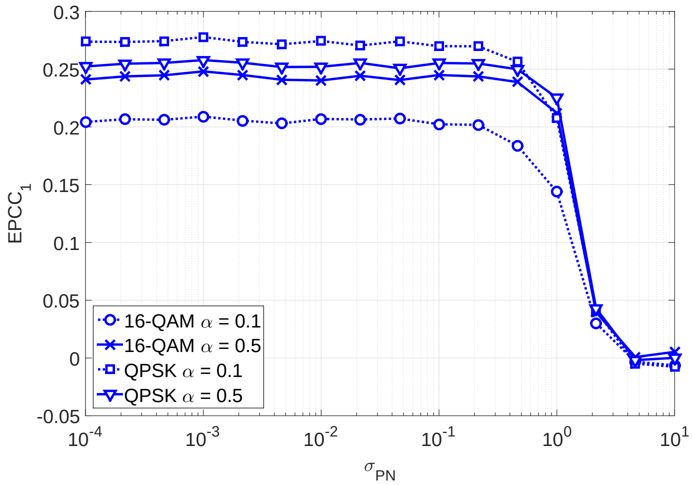

Figure 3: EPCC_1 vs. σ_{PN} for QPSK and 16-QAM.

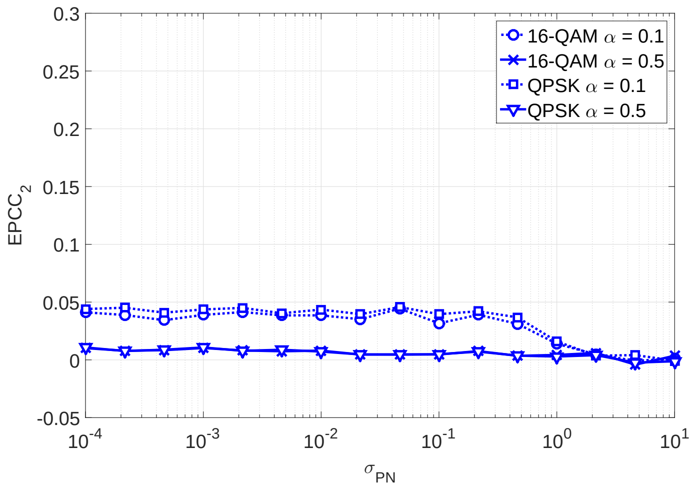

Figure 4: EPCC_2 vs. σ_{PN} for QPSK and 16-QAM.

3.2. Test of Gaussianity

The sequence of N DTFN samples $\{\upsilon_1, \upsilon_2, ..., \upsilon_N\}$ is used to build a histogram $p_\upsilon(x)$ of the samples distribution. In order to test the gaussianity of the DTFN, we compute the Kullback-Leibler (KL) divergence between $p_\upsilon(x)$ and the Gaussian distribution

$$g(x) = \frac{1}{\sqrt{2\pi\sigma^2}} \exp\left(-\frac{x^2}{2\hat{\sigma}_\upsilon^2}\right). \tag{17}$$

The KL divergence provides a measure of the discrepancy between two probability distributions. In [36] Monte-Carlo simulations are presented to demonstrate the superiority of the KL compared to other statistical methods to test gaussianity. The KL divergence formula is

$$\begin{aligned} D_{KL}(p_\upsilon(x)||g(x)) &= \int_{-\infty}^{+\infty} p_\upsilon(x) \ln\left[\frac{p_\upsilon(x)}{g(x)}\right] dx = \\ &= -H(p_\upsilon) - \int_{-\infty}^{+\infty} p_\upsilon(x) \left[-\frac{1}{2}\ln(2\pi\hat{\sigma}_\upsilon^2) - \frac{x^2}{2\hat{\sigma}_\upsilon^2}\right] dx = \\ &= -H(p_\upsilon) + \frac{1}{2}\ln(2\pi\hat{\sigma}_\upsilon^2) + \frac{1}{2}\frac{\hat{\sigma}_\upsilon^2}{\hat{\sigma}_\upsilon^2} = \\ &= -H(p_\upsilon) + \frac{1}{2}\ln(2\pi e\hat{\sigma}_\upsilon^2) = H(g) - H(p_\upsilon), \end{aligned} \tag{18}$$

where $H(p_z)$ denotes the entropy of the random process z with probability density function $p_z(x)$. Simulations were carried out for QPSK and 16-QAM constellations. Figure 5 reports the KL divergence in nats versus σ_{PN} for $\alpha = 0.1$. For each point in the plots the histogram is built with 10^3 bins and $N = 2 \cdot 10^5$.

3.3. Discussion about Whiteness and Gaussianity

Values of $D_{KL}(p_\upsilon(x)||g(x)) \simeq 0$ mean that $\{\upsilon_i\}$ is virtually Gaussian. From Fig. 5 we observe that this happens for values of σ_{PN} lower than the threshold value $\overline{\sigma}_{PN} \simeq 0.3\,\text{rad}$. From the Figure it is clear that the KL divergence measured for σ_{PN} below the threshold $\overline{\sigma}_{PN}$ is never greater than 0.04. Above $\overline{\sigma}_{PN}$

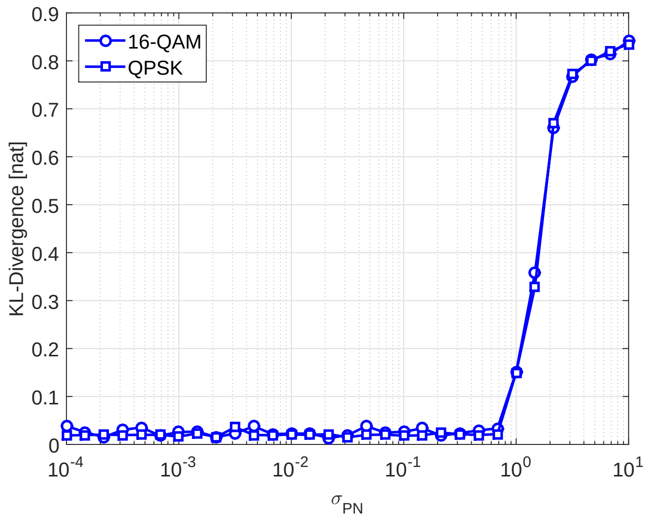

Figure 5: KL divergence vs. σ_{PN} for QPSK and 16-QAM transmission.

the discrete-time frequency noise cannot be considered Gaussian. This means that if the phase noise is too strong then the approximation of the CTWSMF with the DTW does not hold anymore.

A completely different behavior can be observed in Fig. 3 for EPCC_1: when $\sigma_{PN} > \overline{\sigma}_{PN}$ EPCC_1 tends to 0. This would lead us to the conclusion that the phase noise of the CTWSMF cannot be approximated to a discrete-time Wiener process, at least for small values of σ_{PN}. **However, Secs. 4 and 5 will enlighten that the difference between the non-white discrete-time frequency noise υ_i, obtained from simulations, and the discrete-time white frequency process, defining the random increment of the Wiener phase noise in (5), does not have any significant impact on the power of the error associated with the mismatch due to the use of the two models and on the associated measured BERs. As a consequence, the non-whiteness of the discrete-time phase noise can be neglected in practical cases.**

4. Analysis of the Mismatch

The impact of the approximation provided by DTW is analyzed by measuring the mean-squared error

$$P = E[|x_i - a_i e^{j\varphi_i}|^2], \tag{19}$$

where x_i and φ_i are obtained as in Fig. 2. Also, we measure the mean-squared error with non-white frequency noise

$$P_F = E[|x_i - a_i e^{j\varphi_{F,i}}|^2] \tag{20}$$

with

$$\varphi_{F,i} = \angle(z_1 e^{j\varphi_{i-1}} + e^{j\varphi_i} + z_1 e^{j\varphi_{i+1}})$$

where z_1 is the correlation coefficient EPCC_1. From Figs. 6 and 7 one can notice that **for both the two considered roll-off values** P and P_F scale with respect to σ_{PN} with a 20 dB/decade slope up to about 0.3 rad. By comparing Figs. 6 and 7 one realizes that $10\log_{10}(P/P_F) \simeq 1\,\mathrm{dB}$. This small difference means that the memory in the DTFN does not dominate the quality of the approximation. Also more important to note is that, with σ_{PN} smaller than 0.1 rad, the powers of the errors P and P_F are still very low, being more than 20 dB below the signal power. It should be said that $\sigma_{PN} = 0.1$ rad is really strong phase noise, which can be tolerated only by robust systems as coded BPSK or coded QPSK. **Since the threshold SNR for these systems is typically below 10 dB, we can conclude that for both the two models the level of the error power due to phase noise mismatch is much lower than that due to AWGN.** This makes negligible the impact of the mismatch introduced by DTW on system performance.

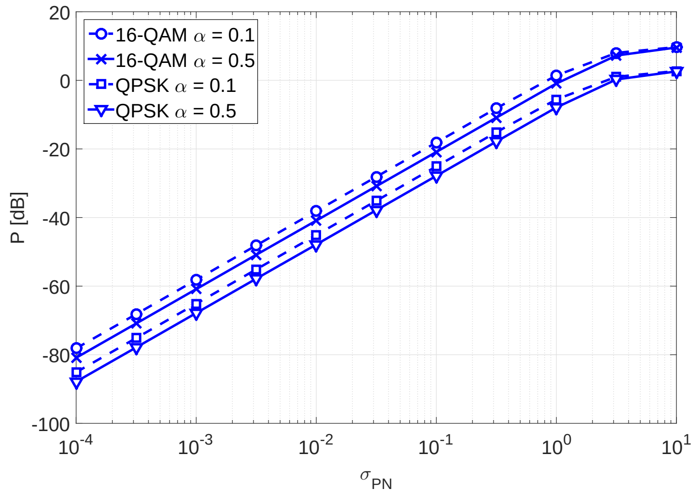

Figure 6: P vs. σ_{PN} in the case of QPSK and 16-QAM transmission.

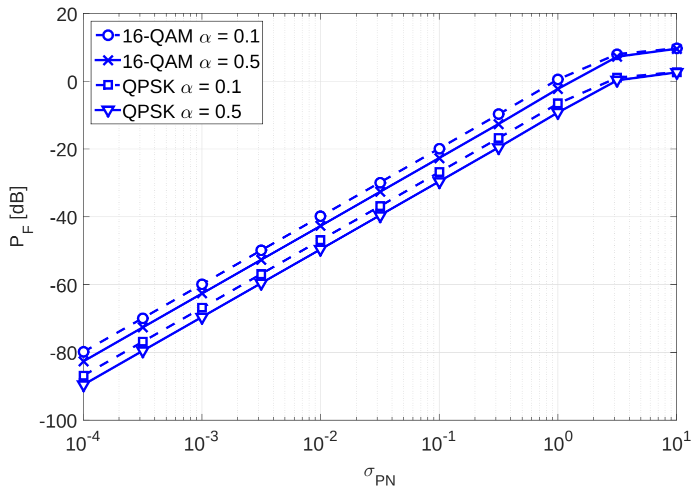

Figure 7: P_F vs. σ_{PN} in the case of QPSK and 16-QAM transmission.

5. BER Performance and Phase Noise Power Spectral Densities Comparison

To validate the accuracy of the approximation provided by the DTW channel model, we use computer simulations to compare its BER with that obtained by using the CTWSMF channel model in case of coherent detection of QPSK and 16-QAM. For DTW the discrete-time signals are generated according to eqns. (4) and (5), while for the CTWSMF they are generated according to the scheme reported in Fig. 2. The BER with the CTWSMF channel model is measured

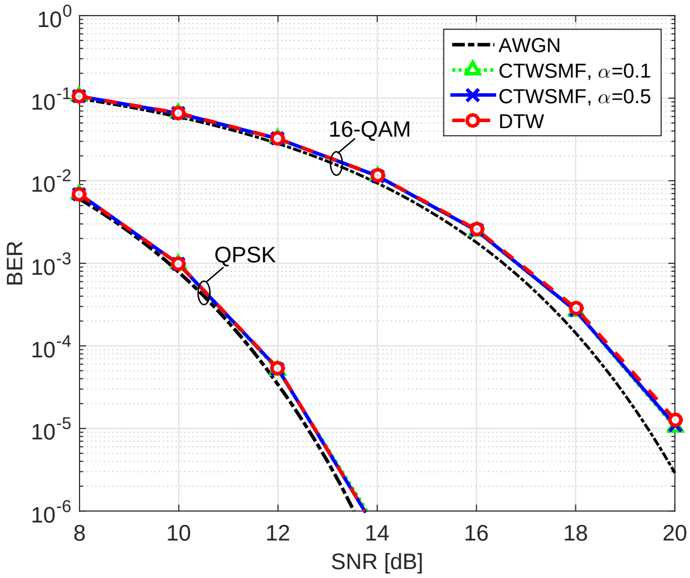

Figure 8: BER vs. SNR for QPSK and 16-QAM with σ_{PN}=$3 \cdot 10^{-2}$.

for $\alpha = 0.1$ and $\alpha = 0.5$. As standard deviation values we consider σ_{PN} equal to $3 \cdot 10^{-2}$ rad, $6.6 \cdot 10^{-2}$ rad, and 0.135 rad. These values can be considered as representative of channels that are characterized by phase-noise levels of practical interest [34, 37]. It is worth noting that, only $\sigma_{PN} = 3 \cdot 10^{-2}$ and $\sigma_{PN} = 6.6 \cdot 10^{-2}$ are below the threshold of 0.1 rad that defines the maximum standard deviation for which a good agreement has been observed in the previous Sections between the statistical tests applied to the two models **and for which the mean-squared error due to the mismatch is below 20 dB.**

Coherent demodulation of the discrete-time received sequence is realized by the pilot-aided trellis scheme proposed in [13]. Such a method is able to provide good tolerance to phase noise because it implements virtually optimal Bayesian tracking of the unknown phase. It relies on the insertion of known pilot symbols that are time-division multiplexed with the information-bearing symbols. In the results shown in this Section we use a pilot overhead of 5%.

Figure 8 reports the BER versus SNR for $\sigma_{PN} = 3 \cdot 10^{-2}$. An excellent fit is found between the BER curves of the two models. The AWGN performance is also reported as a reference in the Figure. For $\sigma_{PN} = 6.6 \cdot 10^{-2}$ the measured BERs are shown in Figure 9. In this case we observe that for QPSK we still have a good agreement between the two models, while, in contrast, for 16-QAM a small deviation appears at BER values lower than 10^{-3}, being the performance achieved by DTW slightly worse than that achieved by CTWSMF. Figure 10 shows results for $\sigma_{PN} = 0.135$. Due to strong phase noise, for both the two models a BER floor is observed at high SNR with 16-QAM. The DTW channel model exhibits a BER floor that is one order of magnitude lower than that of

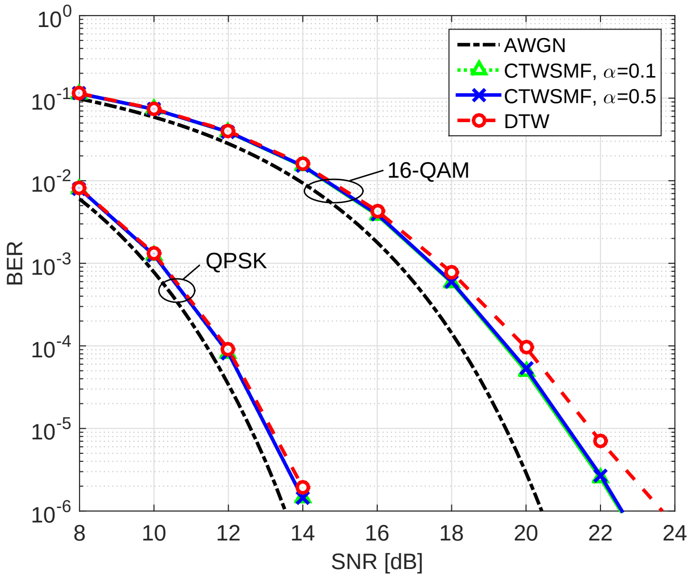

Figure 9: BER vs. SNR for QPSK and 16-QAM with σ_{PN}=$6.6 \cdot 10^{-2}$.

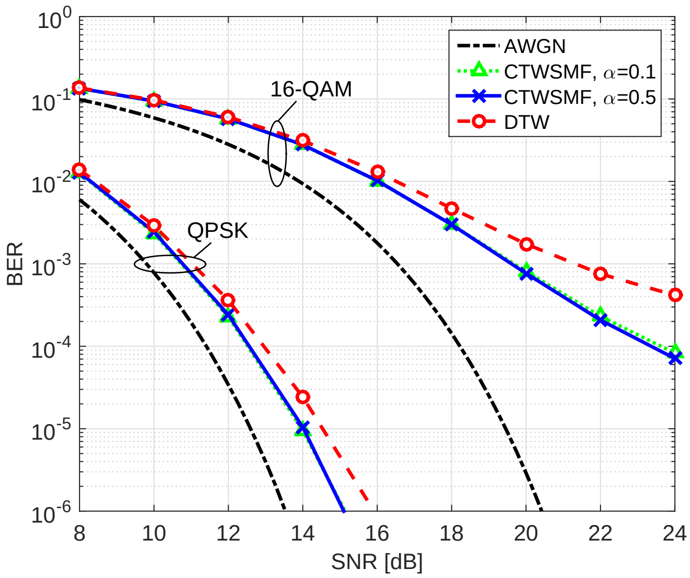

Figure 10: BER vs. SNR for QPSK and 16-QAM with $\sigma_{PN} = 0.135$.

DTW. From these results we conclude that when the DTW channel model is used in computer simulations the resulting BER measure is always conservative. Also, we observe that in all the considered cases the roll-off factor has negligible

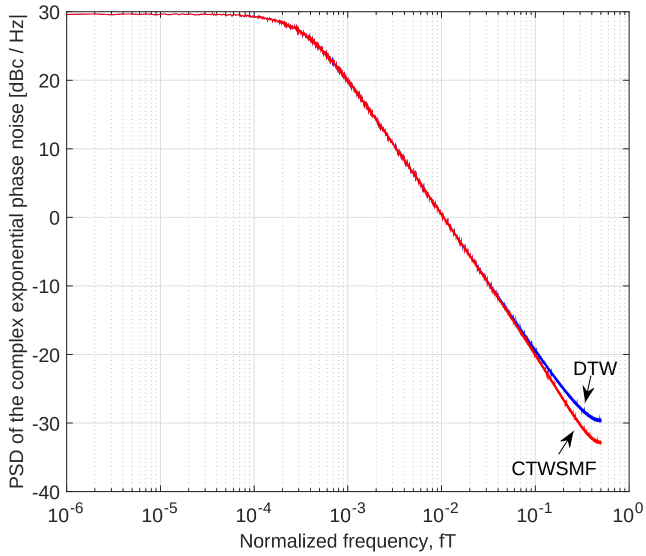

Figure 11: Power spectral density of the discrete-time complex exponential phase noise with σ_{PN}=$6.6 \cdot 10^{-2}$.

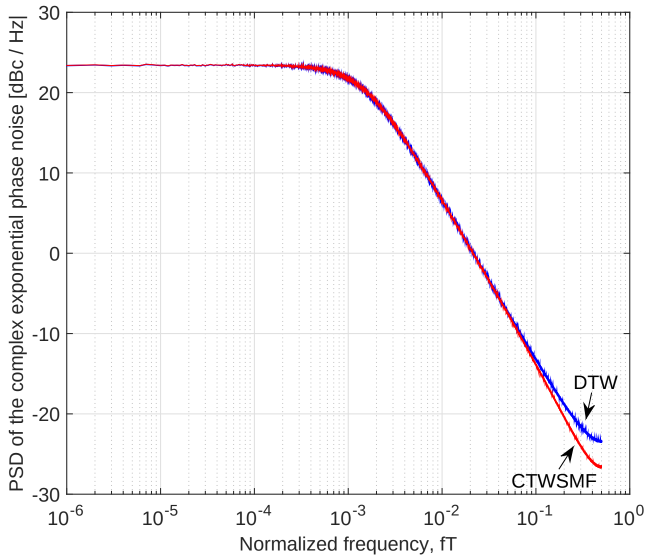

Figure 12: Power spectral density of the discrete-time complex exponential phase noise with σ_{PN}=0.135.

impact on the BER performance achieved by using CTWSMF.

The difference of performance between the two models can be explained by analyzing the phase noise spectra. Figures 11 and 12 show the power spectral density of the complex exponential function of the discrete-time phase noise for the DTW and CTWSMF with $\alpha = 0.1$ for $\sigma_{PN} = 6.6 \cdot 10^{-2}$ and $\sigma_{PN} = 1.35 \cdot 10^{-1}$, respectively. **The reason for choosing $\alpha = 0.1$ is motivated by the numerical results shown in Figs. 6 and 7, where it is shown that for such a value of roll-off the power of the mismatch is higher than that achieved by $\alpha = 0.5$ for both CTWSMF and DTW.** From Figs. 11 and 12 it can be seen that the spectrum of discrete-time phase noise of CTWSMF is narrower than the spectrum of phase noise of DTW, the difference between the two being apparent for normalized frequency greater than 10^{-1}. This difference can be explained by observing that CTWSMF has been sampled after having been filtered through the matched filter, which increases the duration of the continuous-time phase noise memory thus narrowing the spectrum. It is strongly intuitive that the phase noise with narrower spectrum can be better tracked than the one with broader spectrum. From the performance reported in Figs. 9 and 10 we come to the conclusion that the benefit due narrower phase noise spectrum exceeds the loss due to ISI.

6. Conclusion

We have analyzed the differences between the symbol-spaced discrete-time channel model that is commonly adopted to evaluate performance degradation introduced by discrete-time multiplicative Wiener phase noise and the more accurate model obtained by filtering and sampling at symbol-rate the continuous-time received signal affected by multiplicative continuous-time Wiener phase noise. The fit between the two models has been analyzed by means of statistical tests aiming to verify temporal and distributional properties. We have considered the power of the error resulting from the mismatch of the noiseless signals between the two models. We have found that, when the standard deviation of the discrete-time Wiener phase-noise increment is below 0.1 rad, a range of values that are often met in real systems, the discrete-time model provides a good approximation to the sampled filtered model with continuous-time phase noise with the same width of the spectral line, being the power of the error about 20 dB below that of the signal. The good quality of the approximation is also demonstrated by analysis of error performance, showing that BERs of QPSK and 16-QAM are close to each other for the two models. This indicates that, for these systems, one can skip the continuous-time model and consider only the symbol spaced model of equations (4) and (5).

References

[1] P. Leoni, V. Sleiffer, S. Calabrò, M. Kuschnerov, S. Jansen, B. Spinnler, B. Lankl, On the performance of a soft decision FEC scheme operating in highly non-linear regime, in: Signal Processing in Photonic Communications, Optical Society of America, 2012, pp. SpTu3A–6.

[2] M. Maurizio, L. Barletta, A. Spalvieri, A. Leven, M. Pepe, G. Gavioli, Impact of non-ideal phase reference on soft decoding of differentially encoded modulation, IEEE Photon. Technol. Lett. 24 (23) (2012) 2179–2182.

[3] B. Goebel, R.-J. Essiambre, G. Kramer, P. J. Winzer, N. Hanik, Calculation of mutual information for partially coherent Gaussian channels with applications to fiber optics, IEEE Trans. Inf. Theory 57 (9) (2011) 5720–5736.

[4] G. J. Foschini, G. Vannucci, Characterizing filtered light waves corrupted by phase noise, IEEE Trans. Inf. Theory 34 (6) (1988) 1437–1448.

[5] R.-J. Essiambre, G. Kramer, P. J. Winzer, G. J. Foschini, B. Goebel, Capacity limits of optical fiber networks, J. Lightw. Technol. 28 (4) (2010) 662–701.

[6] G. Colavolpe, Communications over phase noise channels: a tutorial review, Int. J. Satell. Commun. Netw. 32 (3) (2014) 167–185.

[7] T. Pfau, S. Hoffmann, R. Noé, Hardware-efficient coherent digital receiver concept with feedforward carrier recovery for M-QAM constellations, J. Lightw. Technol. 27 (8) (2009) 989–999.

[8] S. O. Zafra, X. Pang, G. Jacobsen, S. Popov, S. Sergeyev, Phase noise tolerance study in coherent optical circular QAM transmissions with Viterbi-Viterbi carrier phase estimation, Opt. Express 22 (25) (2014) 30579–30585.

[9] M. Morsy-Osman, Q. Zhuge, L. R. Chen, D. V. Plant, Feedforward carrier recovery via pilot-aided transmission for single-carrier systems with arbitrary M-QAM constellations, Opt. Express 19 (2011) 24331–24343.

[10] F. Zhang, Y. Li, J. Wu, W. Li, X. Hong, J. Lin, Improved pilot-aided optical carrier phase recovery for coherent M-QAM, IEEE Photon. Technol. Lett. 24 (2012) 1577–1580.

[11] A. Spalvieri, L. Barletta, Pilot-aided carrier recovery in the presence of phase noise, IEEE Trans. Commun. 59 (2011) 1966–1974.

[12] M. Magarini, L. Barletta, A. Spalvieri, F. Vacondio, T. Pfau, M. Pepe, M. Bertolini, G. Gavioli, Pilot-symbols-aided carrier-phase recovery for 100-G PM-QPSK digital coherent receivers, IEEE Photon. Technol. Lett. 24 (2012) 739–741.

[13] L. Barletta, F. Bergamelli, M. Magarini, N. Carapellese, A. Spalvieri, Pilot-aided trellis-based demodulation, IEEE Photon. Technol. Lett. 25 (2013) 1234–1237.

[14] T. Koike-Akino, K. Kojima, D. Millar, K. Parsons, Y. Miyata, W. Matsumoto, T. Mizuochi, Cycle slip-mitigating turbo demodulation in LDPC-coded coherent optical communications, in: O. S. of America (Ed.), Optical Fiber Communication Conference, Vol. 59, 2014, pp. M3A–3.

[15] T. Yoshida, T. Sugihara, K. Ishida, T. Mizuochi, Cycle slip compensation with polarization block coding for coherent optical transmission: two-dimensional phases constellation corresponds to a slip state, IEEE Sig. Proc. Mag. 31 (2014) 57–69.

[16] L. Liu, L. Li, Cycle-slip correction in 100Gb/s PM-QPSK systems, in: O. S. of America (Ed.), Conference on Optical Fiber Communication, Technical Digest Series, Vol. 59, 2014.

[17] H. Cheng, Y. Li, M. Yu, J. Zang, J. Wu, J. Lin, Experimental demonstration of pilot-symbols-aided cycle slip mitigation for QPSK modulation format, in: O. S. of America (Ed.), Optical Fiber Communication Conference, 2014, pp. Th4D–1.

[18] H. Cheng, Y. Li, F. Zhang, J. Wu, J. Lu, G. Zhang, J. Lin, Pilot-symbols-aided cycle slip mitigation for DP-16QAM optical communication systems, Opt. Express 21 (19) (2013) 22166–22172.

[19] M. Y. Leong, K. J. Larsen, G. Jacobsen, S. Popov, D. Zibar, S. Sergeyev, Dimensioning BCH codes for coherent DQPSK systems with laser phase noise and cycle slips., J. Lightw. Technol. 32 (21) (2014) 3446–3450.

[20] L. Barletta, M. Magarini, A. Spalvieri, Staged demodulation and decoding, Opt. Express 20 (21) (2012) 23728–23734.

[21] S. T. Le, T. Kanesan, E. Giacoumidis, N. J. Doran, A. D. Ellis, Quasi-pilot aided phase noise estimation for coherent optical OFDM systems, IEEE Photon. Technol. Lett. 26 (2014) 504–507.

[22] J. Dauwels, H. A. Loeliger, Computation of information rates by particle methods, IEEE Trans. Inf. Theory 54 (1) (2008) 406–409.

[23] L. Barletta, M. Magarini, A. Spalvieri, Estimate of information rates of discrete-time first-order Markov phase noise channels, IEEE Photon. Technol. Lett. 23 (21) (2011) 1582–1584.

[24] A. Barbieri, G. Colavolpe, On the information rate and repeat-accumulate code design for phase noise channels, IEEE Trans. Commun. 59 (12) (2011) 3223–3228.

[25] L. Barletta, M. Magarini, A. Spalvieri, A new lower bound below the information rate of Wiener phase noise channel based on Kalman carrier recovery, Opt. Express 20 (2012) 25471–25477.

[26] L. Barletta, M. Magarini, A. Spalvieri, Tight upper and lower bounds to the information rate of the phase noise channel, in: IEEE Intern. Symposium on Inf. Theory, 2013, pp. 2284–2288.

[27] G. Durisi, A. Tarable, C. Camarda, R. Devassy, G. Montorsi, Capacity bounds for MIMO microwave backhaul links affected by phase noise, IEEE Trans. Commun. 62 (3) (2014) 920–929.

[28] M. R. Khanzadi, G. Durisi, T. Eriksson, Capacity of SIMO and MISO phase-noise channels with common/separate oscillators, to appear on IEEE Trans. Commun.

[29] H. Ghozlan, G. Kramer, On Wiener phase noise channels at high signal-to-noise ratio, in: IEEE Intern. Symposium on Inf. Theory, 2013, pp. 2279–2283.

[30] H. Ghozlan, G. Kramer, Multi-sample receivers increase information rates for Wiener phase noise channels, in: IEEE Global Telecommun. Conf. (GLOBECOM), 2013.

[31] L. Barletta, G. Kramer, Lower bound on the capacity of continuous-time Wiener phase noise channels, arXiv preprint arXiv:1503.03223.

[32] L. Barletta, G. Kramer, Signal-to-noise ratio penalties for continuous-time phase noise channels, in: Cognitive Radio Oriented Wireless Networks and Communications, 2014.

[33] H. Schulze, Stochastic models for phase noise, in: Intern. OFDM-Workshop, 2005.

[34] M. Magarini, A. Spalvieri, F. Vacondio, M. Bertolini, M. Pepe, G. Gavioli, Empirical modeling and simulation of phase noise in long-haul coherent optical transmission systems, Opt. Express 19 (23) (2011) 22455–22461.

[35] R. M. Mickey, O. J. Dunn, V. A. Clark, Applied Statistics: Analysis of Variance and Regression, 3rd Edition, Wiley, Hoboken, NJ, 2014.

[36] I. Arizono, H. Ohta, A test for normality based on Kullback–Leibler information, The American Statistician 43 (1) (1989) 20–22.

[37] A. Bisplinghoff, C. Cabirol, S. Langenbach, W. Sauer-Greff, B. Schmauss, Soft decision metrics for differentially encoded QPSK, in: Proc. ECOC, 2011, p. Tu.6.A.2.